Electronic Supplementary Material (ESI) for Physical Chemistry Chemical Physics.

$U@C_{28}$: The Electronic Structure Induced by 32-Electron Principle

Xing Dai[a,b], Yang Gao[a,b], Wanrun Jiang[a,b], Yanyu Lei[a,b] and Zhigang Wang[a,b,*]

[a]*Institute of Atomic and Molecular Physics, Jilin University, Changchun, 130012, People's Republic of China*

[b]*Jilin Provincial Key Laboratory of Applied Atomic and Molecular Spectroscopy (Jilin University), Changchun, 130012, People's Republic of China*

Corresponding Author

* Email: wangzg@jlu.edu.cn

Supporting Information

TABLE OF CONTENTS

level

1. The ground state and electronic structure of C_{28}

Geometric optimizations of T_d C_{28} at PBE/6-31G* level showed C_{28} has a quintet ground state. It can be seen from Figure S1 the spin state of T_d C_{28} is mainly contributed from the $8a_1$ and $14t_2$ orbitals. The $14t_2$ orbital is triplet degenerated, and the MO energy of $8a_1$ is closed to $14t_2$. Therefore, the electronic structure of T_d C_{28} can be described as $(a1)^1(t2)^3$, in agreement with the previous report.

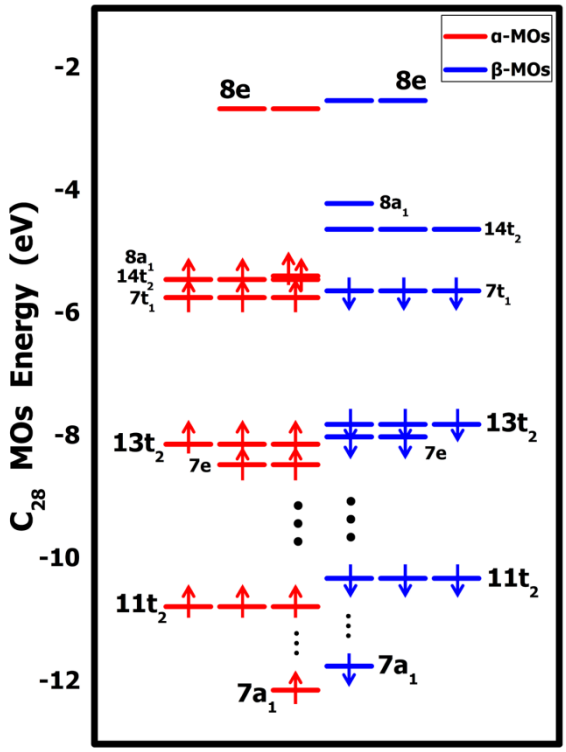

Figure S1. The MOs energy diagram of C_{28} (T_d, Quintet) calculated at PBE/6-31G*.

Among all the occupied MOs of C_{28}, the $8a_1$, $14t_2$, $7t_2$, $13t_2$, 7e, $11t_2$ and $7a_1$ MOs could play crucial roles in hybridizing with actinides, because they have the unique orbital shapes. They are presented in Figure S2.

According to Figure S2, the shapes of $8a_1$, $14t_2$, and $7t_1$ orbitals of C_{28} are similar to those f-type atomic orbitals. Hence, these orbitals are expected to hybridize with 5f atomic orbital of actinides. Similarly, the $13t_2$ and 7e orbitals of C_{28} are favor to hybridize with d-type atomic orbitals. The $11t_2$ and $9a_1$ are beneficial to hybridize with p- and s-type atomic orbitals, respectively.

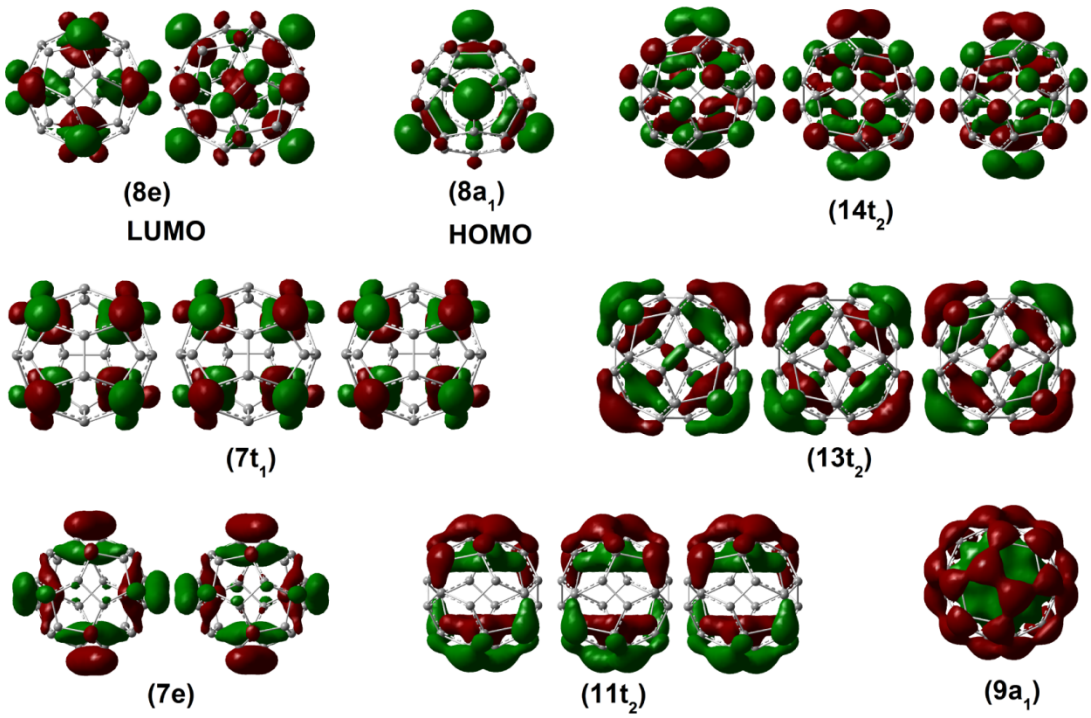

Figure S2. Selected Kohn-Sham α-MOs of C_{28} (T_d, Quintet) calculated at PBE/6-31G* level. The compositions of β-MOs are similar to the corresponding α-MOs. Isosurface = 0.04.

2. The ground state and electronic structure of $[U@C_{28}]^{2+}$

Table S1. Total energy differences of $[U@C_{28}]^{2+}$ at PBE/RECP and B3LYP/RECP levels. The missing data is due to the inexistent electronic states caused by the degenerated frontier MOs at high symmetry.

$[U@C_{28}]^{2+}$	ΔE (eV)					
	PBE			B3LYP		
	Singlet	Triplet	Quintet	Singlet	Triplet	Quintet
T_d	**0**	/	/	**0**	/	/
D_2	**0**	2.63	5.66	**0**	2.76	5.86
D_{2d}	0.04	2.68	5.71	0.03	2.79	5.89
C_{2v}	0.04	2.68	5.71	0.03	2.79	5.89
C_2	0.04	2.68	5.71	0.03	2.79	5.90
C_s	0.03	2.68	5.71	0.03	2.79	5.90

From Table S1, the (T_d, Singlet) state of $[U@C_{28}]^{2+}$ has the lowest total energy. The electronic states of (D_2, Singlet) and (T_d, Singlet) are isoenergetic. Similarly, Table S1 also shows that the C_{2v}, C_2 and C_s symmetries are isoenergetic with D_{2d}.

The total energy of (D_{2d}, Singlet) is slight higher than (T_d, Singlet) and (D_2, Singlet). In order to confirm the real ground state, geometric optimizations for these three electronic states were further performed using different exchange-correlation

functionals. Here, the widely used eight functionals were employed (see Table S2).

Table S2. Total energy differences of three low-lying electronic states of $[U@C_{28}]^{2+}$ at DFT/RECP levels.

$[U@C_{28}]^{2+}$	ΔE (eV)		
	(T_d, Singlet)	(D_2, Singlet)	(D_{2d}, Singlet)
LSDA	0	0	0.05
PBE	0	0	0.04
(+ZPE)	(0)	(0)	(0.02)
PW91	0	0	0.04
BP86	0	0	0.04
BLYP	0	0	0.03
B3LYP	0	0	0.03
PBE0	0	0	0.04
HSE06	0	0	0.04

From Table S2, all the selected functionals suggest that the electronic state (T_d, Singlet) has the lowest total energy. Therefore, $[U@C_{28}]^{2+}$ has a closed-shell ground state with T_d symmetry, in agreement with the previous report.

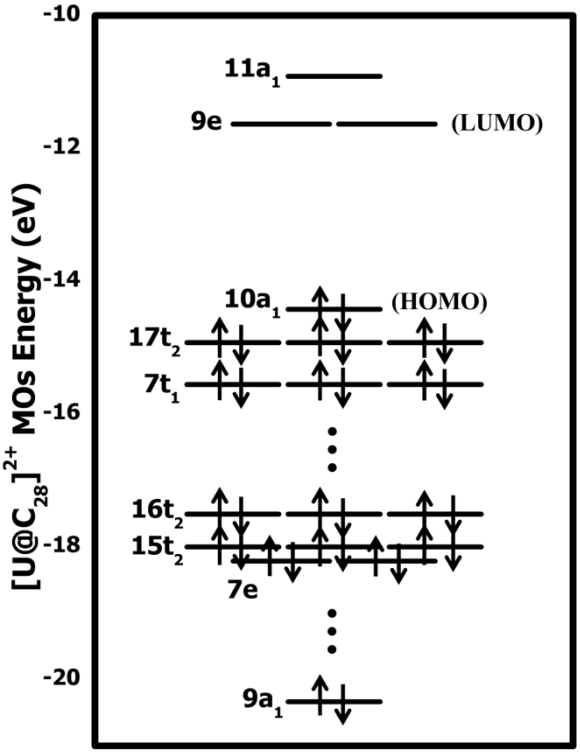

Figure S3. The MOs energy diagram of $[U@C_{28}]^{2+}$ (T_d, Singlet) calculated at PBE/RECP level. The neglected MOs are from pure C_{28} cage contribution.

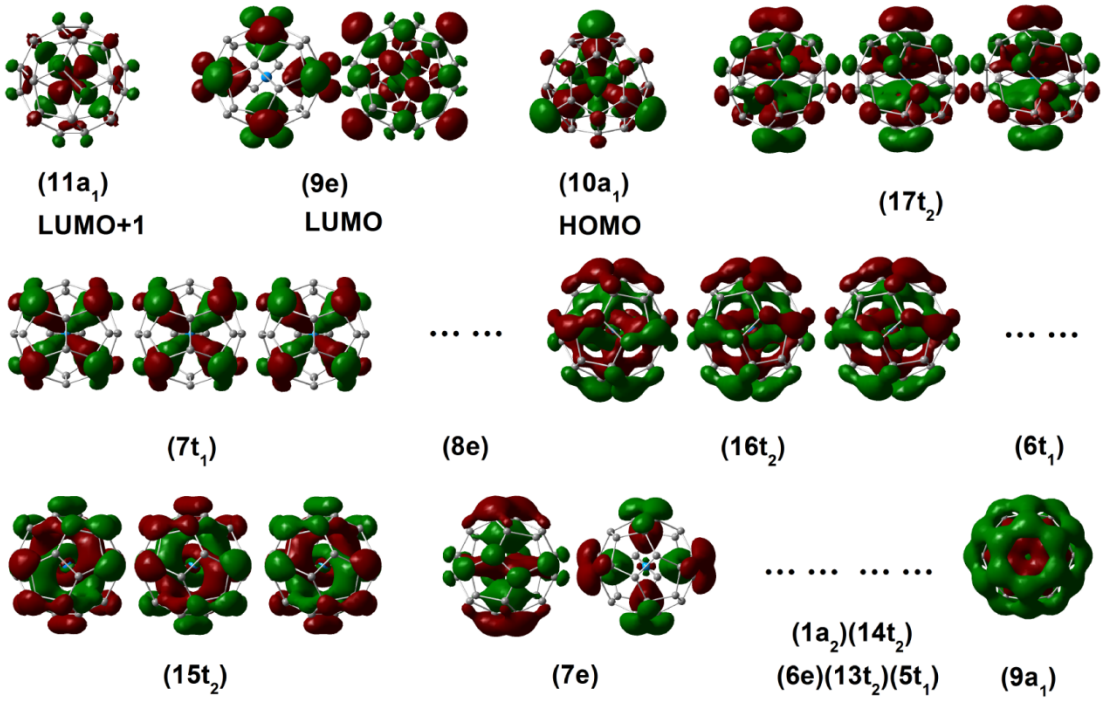

Figure S4. Selected Kohn-Sham α-MOs of $[U@C_{28}]^{2+}$ (T_d, Singlet) calculated at PBE/RECP level. The compositions of β-MOs are similar to the corresponding α-MOs. The neglected MOs are pure C_{28} cage orbitals. Isosurface = 0.035.

Table S3. The orbital compositions of $[U@C_{28}]^{2+}$ (T_d, Singlet).

MOs	Occ.	Orbital compositions				
		U-5f	U-6d	U-7p	U-7s	Cage
9e	0					100%
$10a_1$	2	24.87%				75.13%
$17t_2$	6	26.01%				73.99%
$7t_1$	6	23.15%				76.85%
$16t_2$	6		3.95%	8.95%		87.10%
$15t_2$	6		5.01%	6.26%		88.73%
7e	4		11.60%			88.40%
$9a_1$	2				6.93%	93.07%

From Figure S3, S4 and Table S3, the $10a_1$, $17t_2$ and $7t_1$ MOs reflect the hybridizations between U-5f orbitals and the cage orbitals. The $16t_2$ and $15t_2$ MOs are contributed from the mixture of U-6d, 7p orbitals and the cage orbitals. The 7e and $9a_1$ MOs correspond to the hybridizations of 6d-cage and 7s-cage, respectively. The electronic configuration of these 32 electrons are consistent with the previous reported $Pu^{4+}@C_{28}$, confirming that the electronic structure of $[U@C_{28}]^{2+}$ satisfies the 32-electron principle, namely 4 electrons from the metal and 28 electrons from the cage should combine to form the 32-electron system. Overall, the uranium and the cage in $[U@C_{28}]^{2+}$ share their 32 valence electrons and all the s-, p-, d-, f-types orbital of U participate in the U-cage covalent bonding.

In addition, the LUMO+1 (i.e. $11a_1$ orbital) has the 5f-π anti-bonding character.

Here, we especially focus on the LUMO, 9e orbital, which is double-degenerated and completely contributed from the cage orbital. The calculated HOMO-LUMO gap at PBE level is about 2.79 eV (see Table S4), in agreement with the previous report. To some extent, this large gap indicates the high stability of the electronic structure. Therefore, it can be expected that the additional electrons for $[U@C_{28}]^{2+}$ may preferentially occupy on its LUMO rather than break the lower-lying stable 32-electron configuration.

Table S4. Geometric parameters and HOMO-LUMO gaps of $[U@C_{28}]^{2+}$ (T_d, Singlet).

$[U@C_{28}]^{2+}$	R_{U-C} (Å)	Gap (eV)
LSDA	2.43, 2.44, 2.49	2.89
PBE	2.46, 2.47, 2.52	2.79
PW91	2.46, 2.47, 2.52	2.78
BP86	2.46, 2.47, 2.52	2.77
BLYP	2.47, 2.48, 2.53	2.68
B3LYP	2.45, 2.46. 2.51	3.98
PBE0	2.43, 2.44, 2.49	4.40
HSE06	2.44, 2.45, 2.49	3.66

3. The ground state and electronic structure of U@C_{28}

3.1 Results at DFT/RECP level

Table S5 shows that the (T_d, Triplet) state of neutral $U@C_{28}$ has the lowest total energy. The electronic states of (D_2, Triplet) and (T_d, Triplet) are isoenergetic. Again, the C_{2v}, C_2 and C_s symmetries are isoenergetic with D_{2d}.

Table S5. Total energy differences of $U@C_{28}$ at PBE/RECP and B3LYP/RECP levels. The missing data is due to the inexistent electronic states caused by the degenerated frontier MOs at high symmetry.

$U@C_{28}$	ΔE (eV)					
	PBE			B3LYP		
	Singlet	Triplet	Quintet	Singlet	Triplet	Quintet
T_d	/	**0**	3.28	/	**0**	2.97
D_2	0.05	**0**	3.28	0.11	**0**	2.97
D_{2d}	0.09	0.05	3.33	0.14	0.03	3.00
C_{2v}	0.09	0.05	3.33	0.14	0.03	3.00
C_2	0.09	0.05	3.34	0.14	0.05	2.99
C_s	0.09	0.05	3.33	0.13	0.03	2.99

The total energies of (D_2, Singlet), (D_{2d}, Singlet) and (D_{2d}, Triplet) are slight higher than (T_d, Triplet) and (D_2, Triplet). So, geometric optimizations for these five electronic states were further performed using different exchange-correlation functionals to confirm the real ground state. From Table S6, all these selected methods suggest that the (T_d, Triplet) is the ground state of neutral U@C_{28}.

Table S6. Total energy differences of five low-lying electronic states of U@C_{28} at DFT/RECP levels.

U@C_{28}	ΔE (eV)				
	(T_d, Triplet)	(D_2, Singlet)	(D_2, Triplet)	(D_{2d}, Singlet)	(D_{2d}, Triplet)
LSDA	0			0.05	0.05
PBE	0	0.05	0	0.09	0.05
(+ZPE)	(0)	(0.04)	(0)	(0.06)	(0.02)
PW91	0	0.05	0	0.10	0.05
BP86	0	0.05	0	0.09	0.05
BLYP	0	0.04	0	0.08	0.04
B3LYP	0	0.11	0	0.14	0.03
(+ZPE)	(0)	(0.11)	(0)	(0.13)	(0.02)
PBE0	0	0.15	0	0.19	0.04
HSE06	0	0.15	0	0.19	0.04

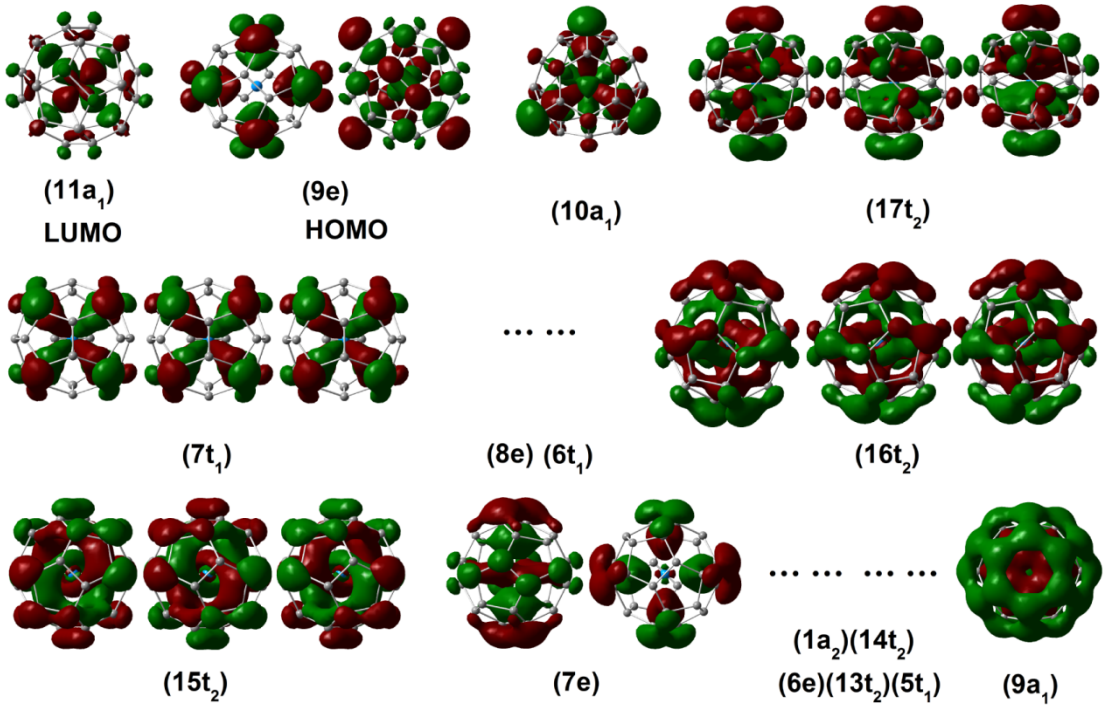

Figure S5. Selected Kohn-Sham α-MOs of U@C_{28} (T_d, Triplet) calculated at PBE/RECP level. The compositions of β-MOs are similar to the corresponding α-MOs. The ZORA-PBE result is well in agreement with PBE/RECP result. The neglected MOs are from pure C_{28} cage contribution. Isosurface = 0.035.

Table S7. The orbital compositions of neutral U@C_{28} (T_d, Triplet).

MOs	Occ.	Orbital compositions				
		U-5f	U-6d	U-7p	U-7s	Cage
9e	2					100%
$10a_1$	2	23.69%				76.31%
$17t_2$	6	24.07%				75.93%
$7t_1$	6	19.65%				80.35%
$16t_2$	6		4.97%	7.73%		87.3%
$15t_2$	6		3.29%	7.78%		88.93%
7e	4		11.97%			88.03%
$9a_1$	2				8.10%	91.90%

The previous reported $(5f)^1(cage)^1$ ground state was not obtained from all the DFT methods in this work. Because all DFT calculations show that all the valence layers of U should hybridize with the cage, none localized 5f orbital of U can be found in the occupied orbitals or in the higher unoccupied orbitals. Instead, we can only find corresponding anti-bonding 5f-cage MOs in the unoccupied levels. We have also tried to allot one net spin for U, as well as the cage, to construct a $(5f)^1(cage)^1$ state by considering both ferromagnetic and antiferromagnetic coupling between the two net spins. But these states always turn to $(cage)^2$ state during the self-consistent-field (SCF) process, indicating that the $(5f)^1(cage)^1$ state is not stable.

3.2 Results at scalar and spin-orbital relativistic ZORA levels

From Table S8, geometric optimizations using scalar relativistic ZORA-PBE method showed that the (T_d, Triplet) and (D_{2d}, Triplet) of neutral U@C_{28} have the lowest total bonding energies, and they are close in energies. Furthermore, geometric optimizations using spin-orbital (SO) relativistic ZORA-PBE method showed that the T_d geometry is more stable.

Table S8. Total bonding energies of neutral U@C_{28} calculated at scalar and spin-orbital relativistic ZORA levels. Note: in ADF program, the electrons are allowed to partially occupied on the degenerated MOs, so the bond energy of (T_d, Singlet) can be obtained.

U@C_{28}		Total Bonding Energy (eV)	
		Scalar-ZORA-PBE	SO-ZORA-PBE
T_d	Singlet	-245.92	
	Triplet	**-246.13**	**-255.40**
	Quintet	-242.73	
D_{2d}	Singlet	-246.08	
	Triplet	**-246.13**	-255.35
	Quintet	-242.73	

Considering the spin polarization of the electrons, the spin-unrestricted calculations

were performed at spin-orbital relativistic ZORA level. However, such calculations require the geometric symmetry being abolished. In this work, the obtained T_d and D_{2d} geometries from scalar-ZORA method were used as the initial structures in SO-ZORA geometric optimizations. We find that the optimized structures from SO-ZORA method are still very close to T_d and D_{2d} symmetries (see the geometric coordinates in Part 5).

In spin-unrestricted SO-ZORA calculations, each level can be allocated one electron. However, it is not directly associated with spin-α or spin-β, but rather with the more general Kramer's symmetry. Therefore, we do not need to discuss the multiplicity in SO-ZORA calculations.

The MOs energy diagrams calculated at both scalar-ZORA and SO-ZORA levels are showed in Figure S6. It can be seen that the scalar-ZORA result (Figure S6 left) is consistent with the DFT/RECP result (Figure 1 in the main text).

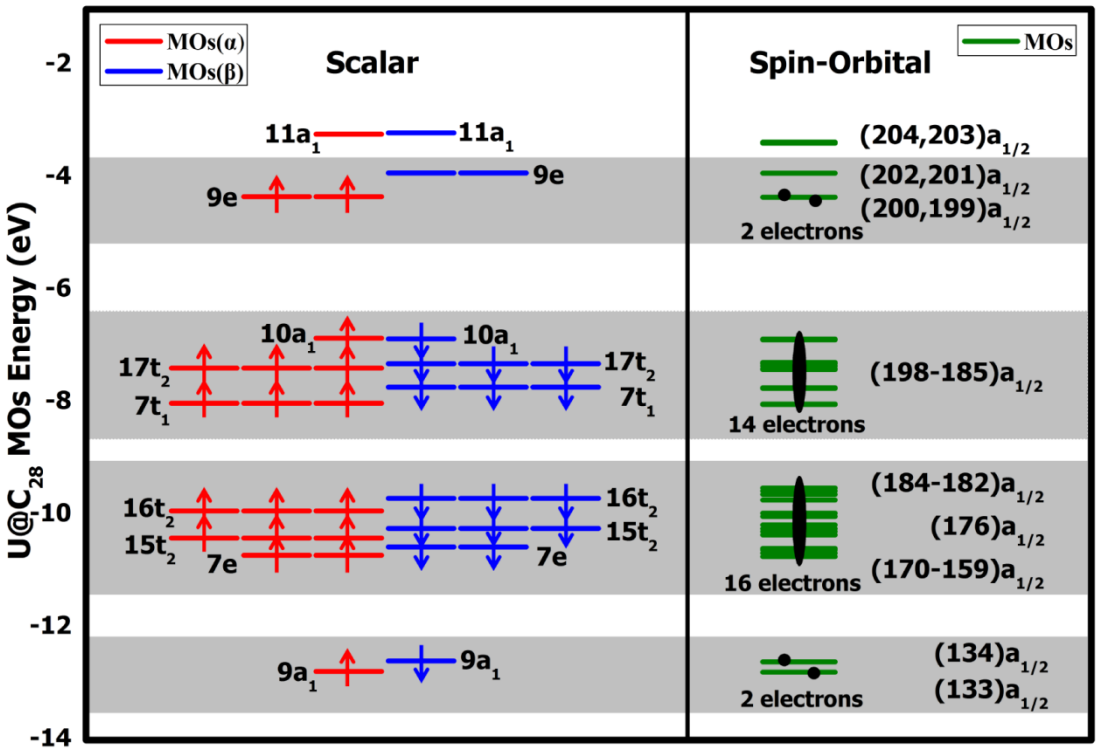

Figure S6. The MOs energy diagram of neutral U@C_{28} calculated at scalar ZORA-PBE (left) and spin-orbital ZORA-PBE (right) levels, respectively. All the irreducible representations of SO-ZORA MOs (right) are a1/2 due to the symmetry was abolished in SO-ZORA calculations. The grey boxes indicate the compositions of the two parts of MOs are comparable.

We should especially note that SO-ZORA calculations also predicted the 32-electron principle. In Figure S6, the 133$a_{1/2}$ and 134$a_{1/2}$ orbitals at spin-orbital level reflect the hybridization of s-type orbital of U and the cage orbitals, corresponding to the 9a_1 orbital at scalar level. The (184-182)$a_{1/2}$, 176$a_{1/2}$ and (170-159)$a_{1/2}$ orbitals showed the

hybridizations among p- and d-type orbitals of U and the cage orbitals, corresponding to the $16t_2$, $15t_2$ and 7e orbitals. The (198-185)$a_{1/2}$ orbitals have the 5f-cage bonding characters, corresponding to the $10a_1$, $17t_2$ and $7t_1$ orbitals.

Most importantly, the $200a_{1/2}$ and $199a_{1/2}$ orbitals are almost degenerated and they are completely contributed from the carbon cage, consistent with the scalar-ZORA prediction (9e orbital). Although we cannot obtain the spin directions in SO-ZORA calculations, it is no doubt that the $(cage)^2$ electronic state of neutral $U@C_{28}$ has been confirmed.

Table S9. Geometric parameters and 9e-$10a_1$ α-gaps of neutral $U@C_{28}$ (T_d, Triplet).

$[U@C_{28}]^{2+}$	R_{U-C} (Å)	9e-$10a_1$ α-Gap (eV)
LSDA	2.42, 2.47, 2.47	2.62
PBE	2.45, 2.49, 2.50	2.45
PW91	2.45, 2.49, 2.50	2.44
BP86	2.45, 2.50, 2.51	2.43
BLYP	2.46, 2.51, 2.52	2.36
B3LYP	2.44, 2.49, 2.49	2.61
PBE0	2.42, 2.47, 2.48	2.72
HSE06	2.43, 2.47, 2.48	2.68
Scalar-ZORA	2.44, 2.49, 2.49	2.51
SO-ZORA	2.44, 2.49, 2.49	2.54 ($199a_{1/2}$-$198a_{1/2}$ gap)

4. The ground state and electronic structure of $[U@C_{28}]^+$

From Table S10 and S11, $[U@C_{28}]^+$ has a (D_2, doublet) ground state.

Table S10. Total energy differences of $[U@C_{28}]^+$ at different geometric symmetries and multiplicities. The missing data is due to the inexistent electronic states caused by the degenerated frontier MOs at high symmetry.

$[U@C_{28}]^+$	ΔE (eV)			
	PBE		B3LYP	
	Doublet	Quartet	Doublet	Quartet
T_d	/	2.62	/	2.75
D_2	**0**	2.62	**0**	2.75
D_{2d}	0.05	2.67	0.03	2.78
C_{2v}	0.05	2.67	0.03	2.78
C_2	0.05	2.66	0.03	2.78
C_s	0.05	2.67	0.03	2.77

Table S11. Total energy differences of two low-lying electronic states of $[U@C_{28}]^+$.

$[U@C_{28}]^+$	ΔE (eV)	
	(D_2, Doublet)	(D_{2d}, Doublet)
LSDA	0	0.06
PBE	0	0.05
PW91	0	0.05
BP86	0	0.05
BLYP	0	0.04
B3LYP	0	0.03
PBE0	0	0.05
HSE06	0	0.05

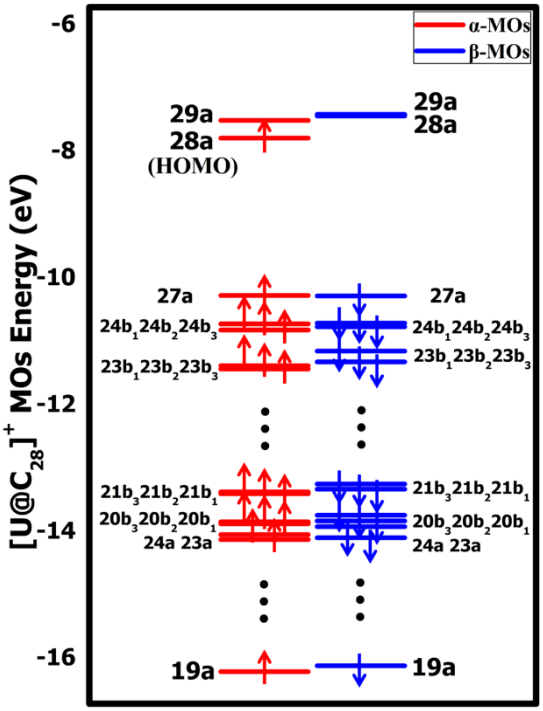

Figure S7. The MOs energy diagram of $[U@C_{28}]^+$ (D_2, Doublet) calculated at PBE/RECP level. The neglected MOs are from pure C_{28} cage contribution.

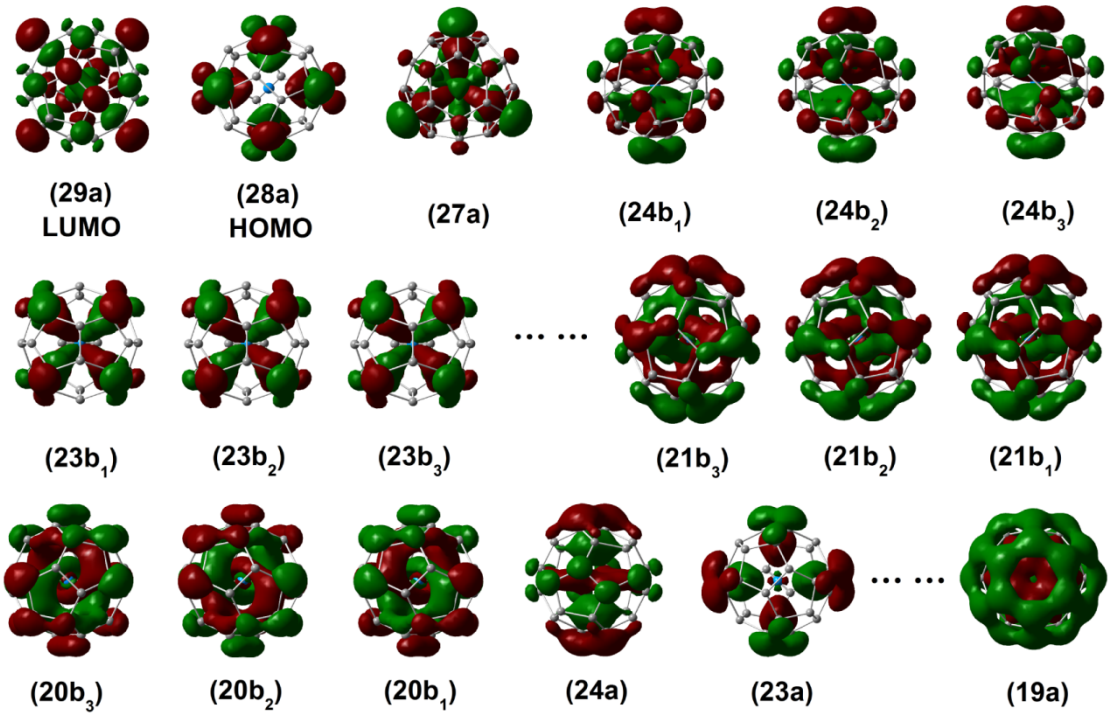

Figure S8. Frontier α-MOs of $[U@C_{28}]^+$ calculated at PBE/RECP level.

Table S12. The orbital compositions of $[U@C_{28}]^+$ (D_2, doublet).

MOs	Occ.	Orbital compositions				
		U-5f	U-6d	U-7p	U-7s	Cage
28a	1					100%
27a	2	24.30%				75.70%
$24b_1$	2	25.63%				74.37%
$24b_2$	2	24.82%				75.18%
$24b_3$	2	24.81%				75.19%
$23b_1$	2	24.11%				75.89%
$23b_2$	2	24.54%				75.46%
$23b_3$	2	21.54%				78.46%
$21b_3$	2		4.18%	8.03%		87.79%
$21b_2$	2		4.18%	8.03%		87.79%
$21b_1$	2		4.25%	8.77%		86.98%
$20b_3$	2		4.06%	7.14%		88.80%
$20b_2$	2		4.06%	7.14%		88.80%
$20b_1$	2		4.57%	6.34%		89.19%
24a	2		11.56%			88.44%
23a	2		11.87%			88.13%
19a	2				7.44%	92.56%

Caused by the Jahn-Teller effect, the last electron of $[U@C_{28}]^+$ could not occupy on the degenerated MOs. So the geometric symmetry should degenerate to D_2. We can see that the 29a and 28a orbitals (i.e. α-LUMO and α-HOMO) of $[U@C_{28}]^+$ are also

completely contributed from the cage, the compositions are similar to the degenerated 9e orbital of neutral $U@C_{28}$. Therefore, the electronic structure of $[U@C_{28}]^+$ can be described as $(cage)^1$.

5. Geometric coordinates of $U@C_{28}$ calculated at spin-orbital ZORA level

Table S13. Optimized T_d geometric coordinates of $U@C_{28}$ at spin-orbital relativistic ZORA level.

Atom	Coordinates (Angstrom)		
	X	Y	Z
C	-1.439392	-1.439390	1.439391
C	1.439390	1.439389	1.439389
C	1.439390	-1.439389	-1.439389
C	-1.439390	1.439389	-1.439390
C	2.324762	0.526793	-0.526793
C	-2.324759	-0.526792	-0.526791
C	-2.324758	0.526791	0.526792
C	2.324761	-0.526791	0.526792
C	0.526792	0.526792	-2.324759
C	-0.526792	0.526791	2.324759
C	0.526791	-0.526792	2.324758
C	-0.526792	-0.526791	-2.324758
C	0.526792	2.324758	-0.526792
C	0.526791	-2.324756	0.526791
C	-0.526792	-2.324758	-0.526792
C	-0.526791	2.324757	0.526791
C	-0.049660	1.757329	-1.757329
C	0.049660	-1.757330	-1.757330
C	0.049660	1.757328	1.757328
C	-0.049661	-1.757331	1.757331
C	1.757333	1.757333	0.049659
C	-1.757331	1.757330	-0.049660
C	1.757330	-1.757329	-0.049660
C	-1.757333	-1.757332	0.049660
C	1.757333	-0.049659	-1.757332
C	1.757332	0.049660	1.757331
C	-1.757333	0.049660	-1.757332
C	-1.757333	-0.049660	1.757333
U	0.000000	0.000000	0.000000

Table S14. Optimized D_{2d} geometric coordinates of U@C_{28} at spin-orbital relativistic ZORA level.

Atom	Coordinates (Angstrom)		
	X	Y	Z
C	1.451027	-1.451027	1.415790
C	-1.451026	1.451025	1.415789
C	1.451026	1.451026	-1.415790
C	-1.451027	-1.451026	-1.415790
C	-0.530818	2.317763	-0.531421
C	0.530818	-2.317762	-0.531421
C	-0.530817	-2.317761	0.531421
C	0.530817	2.317762	0.531421
C	-0.520723	0.520723	-2.339090
C	-0.520724	-0.520724	2.339092
C	0.520723	0.520723	2.339090
C	0.520723	-0.520723	-2.339090
C	-2.317763	0.530818	-0.531421
C	2.317764	0.530818	0.531422
C	2.317762	-0.530818	-0.531421
C	-2.317762	-0.530817	0.531421
C	-1.747964	-0.053330	-1.727830
C	1.747964	0.053331	-1.727830
C	-1.747964	0.053330	1.727829
C	1.747964	-0.053331	1.727830
C	-1.795209	1.795208	0.041977
C	-1.795207	-1.795206	-0.041977
C	1.795208	1.795208	-0.041977
C	1.795208	-1.795208	0.041977
C	0.053330	1.747964	-1.727830
C	-0.053331	1.747962	1.727828
C	-0.053331	-1.747964	-1.727830
C	0.053331	-1.747965	1.727830
U	0.000000	0.000000	0.000000